RSC Advances

PAPER

View Article Online
View Journal | View Issue

Cite this: *RSC Adv.*, 2024, **14**, 1397

Positron scattering from structurally related biomolecules†

Sapna Mahla and Bobby Antony *

We report the integral elastic, momentum transfer, and inelastic (positronium formation and ionisation) cross sections for positron scattering from structurally related molecules. The molecules chosen for the current investigation are formamide, formylphosphine, formic acid, *N*-methylformamide, acetone, acetic acid, and formaldehyde. The cross sections were calculated using the optical potential approach and the complex scattering potential-ionisation contribution method for impact energies between 1 and 5 keV. A sizable repository of data is now available for positron scattering from various atoms and molecules; however, data on the impact of positrons on current targets is still scarce and fragmented. While most cross sections are the first of their kind, we analyze our total cross sections (TCSs) with the previous literature available, which has become attractive to researchers trying to model the tracks of charged particles in matter. TCSs have recently seen a resurgence in popularity thanks to their utility in specifying the mean-free path between the collisions of such simulations. We find good qualitative convergence between experimental and theoretical results below and above the positronium formation threshold. However, around the threshold region, a significant discrepancy is encountered, which can be accounted for due to the experiment's lack of forward angle scattering effect discrimination. This level of agreement evolves to become quantitative at intermediate and higher energies.

Received 13th September 2023
Accepted 19th December 2023

DOI: 10.1039/d3ra06227a

rsc.li/rsc-advances

1 Introduction

Positron (e^+) scattering from atoms or molecules comprises a very intriguing physics that should be carefully reviewed for experiments and theoretical studies in condensed matter, atomic, molecular, and high-energy physics.[1,2] Yet, there is no meticulous and comprehensive investigation of molecular targets. Although many applications based on the impact of positrons on materials have been designed and used frequently, especially in e^+ – microscopy and positron emission tomography (PET),[3,4] not much is comprehended about the fundamentals of e^+ – scattering interactions from gaseous targets. For instance, scientists have theorised that positrons might establish a resonance or adhere to it when interacting with atoms or molecules.[5,6] But there hasn't been any strong scientific proof of this resonance or attachment. Regarding the theoretical aspect, it has not been thoroughly investigated whether positrons can create a molecule-bound condition[7] since the e^+ interaction weakens in comparison to the e^- counterpart. Thus, any theoretical computation relies heavily on the proposed interaction model. Because of this, performing high-precision computational calculations on molecules is highly challenging and remains largely difficult.

Several research groups have used Monte Carlo (MC) simulation methods to investigate particle trails as they move through materials. The ultimate goal of these investigations is to describe how radiation damage manifests in matter at the nanoscale, and the vast majority of them necessitate a substantial data source for the pertinent atomic and molecular processes taking place. A database of this kind demands a high degree of precision and reliability. One such component of this database is the TCS, which is crucial since it determines the mean free path (MFP) during the operation of such simulations between the collisions and, in general, the odds of a collision occurring.[8] To date, the atomic and molecular physics community has concentrated on compounds that might be thought of as analogues, or prototypes, for the "building blocks" of DNA or nucleic acids. The members of this community are united in their support of a reductionist ideology where a system's chemical, biological, and physical traits come from the basic properties of its components and how they interact with each other.[9] Moreover, after the momentous foundation laid in 2000 by Boudaiffa *et al.*[10] for the impact of ionizing radiation on biological molecules, much theoretical and experimental work has shifted its focus to e^+/e^- scattering from biomolecules. While an extensive compilation of experimental and theoretical literature for e^+ – scattering[11,12] from diverse compounds is now available, there is still a shortage of

Department of Physics, Indian Institute of Technology (ISM), Dhanbad, JH 826004, India. E-mail: bobby@iitism.ac.in

† Electronic supplementary information (ESI) available: Numerical cross-section data for present targets (PDF). See DOI: https://doi.org/10.1039/d3ra06227a

positron impact data from present targets, especially for inelastic cross sections. As a consequence, we began an investigation to explore positron interactions with present targets to provide cross-sectional data for researchers interested in studying the behavior of positron swarm transit in different gases[13,14] and simulating the paths of charged particles through matter.[15,16]

In this work, the positron-impact cross sections of formamide ($HCONH_2$), formylphosphine ($HCOPH_2$), formic acid (HCOOH), *N*-methylformamide ($HCONHCH_3$), formaldehyde (HCOH), acetone (CH_3COCH_3), and acetic acid (CH_3COOH) are predicted between 1 and 5 keV on the energy scale. Formamide[17] and its derivative (*N*-methylformamide) are the primary building blocks in the evolution of nucleic acids. They are found in the gaseous phase of the long-period meteorite Hale–Bopp,[18] the interstellar medium (ISM), and the grains surrounding the young interstellar entity W33A.[19] The ubiquitous formamide in interstellar space has an isovalent analogue that can be represented by $HCOPH_2$. Frigge *et al.*[20] suggested that formylphosphine might be present in the ISM, ultimately providing the missing connection between phosphorus-containing compounds detected in the ISM and on comet 67P/Churyumov–Gerasimenko. Formic acid is the most basic organic acid and is believed to be significant in acetic acid production. Both formic and acetic acids can be considered the simplest building blocks of complicated biological compounds, such as DNA nucleotides and amino acids. Acetone is the fundamental aliphatic and carbonyl compound,[21] serving as a solvent and precursor for chemistry polymers. It has been proven a valuable biomarker for diabetic patients[22] and has applications in the ISM. Similarly, formaldehyde is another hydrocarbon with a carbonyl (C═O) group in its chemical structure. The carbonyl functional group is a universal building block in various chemical substances, including polymers such as polyethylene terephthalate, polymethyl methacrylate, and polycarbonate.[23] For such reasons, present targets are not only prime candidates for benchmarking future theoretical advancements but also an acknowledgement of the crucial part performed by the carbonyl group in e^+ – scattering dynamics.

Previous experimental and theoretical studies on e^+ – scattering with the present targets are limited. Those available primarily focus on e^- – collisions.[24–28] Among previous work in the literature for e^+ – HCOOH scattering, we note: (1) the measurements of the total cross sections (Q_{total}) from Kimura *et al.*,[29] who employed a magnetically directed beam in a time-of-flight instrument to determine Q_{total} over the energy range 0.7–600 eV, (2) Makochekanwa *et al.*,[30] who used a e^+ beam with a 60 meV energy resolution (FWHM) to measure Q_{total} and positronium (Ps) formation cross sections (4–60 eV), and (3) Zecca *et al.*[31] who used a magnetic and electrostatic field experimental setup to find Q_{total} within an energy range of 0.3 to 50.2 eV. As for the experimental literature on acetone, Zecca *et al.*[32] and Kimura *et al.*,[29] reported total cross sections over the energy ranges 0.2–23 and 0.7–600 eV, respectively. Another source of available data on Q_{total} for e^+ – acetone scattering is from Hamada *et al.*[33] Regarding the experimental data on formaldehyde, the only data accessible are from Zecca *et al.*[34] for Q_{total} in the energy range of 0.26 and 50.3 eV. Theoretically, there are two previous works in the literature on e^+ – scattering from formic acid and formaldehyde, involving computations of elastic integral (Q_{el}) cross sections using the Schwinger multichannel method (SMC), a collaborative publication with the experimental results of Zecca *et al.*[31,34] For formamide and acetone, only the investigations of low-energy e^+ – scattering from Silva *et al.*[35] and Lima *et al.*[21] are available. The authors have used the SMC method to calculate Q_{el} for impact energies up to 10 eV.

To the best of our knowledge, no other theoretical or experimental literature is available on positron scattering from these targets. From a theoretical point of view, this shows how hard it is to give a precise explanation of quantum collisions, especially to include Ps formation in the formalistic framework. Thus, more advancements in experimental approaches and scattering models are desirable. To partially fill the gap in e^+ – scattering data and to provide an organized analysis of the results that are currently accessible in the literature, we report calculations of elastic (Q_{el}), momentum transfer (Q_{mtcs}), total ionisation ($Q_{ion} + Q_{ps}$), and total (Q_{total}) cross sections within the scope of energy from 1 eV to 5 keV. Besides that, the total inelastic cross sections for positronium formation (Q_{ps}), direct ionisation (Q_{ion}), and electronic excitations (Q_{exc}) are also given. These cross sections are important in models of e^+ transport because they allow monitoring of the positrons' energy as they dissipate into the medium and facilitate the generation of secondary electrons.[36] Furthermore, we investigate whether any patterns exist in the energy dependencies of the e^+ impact cross sections of the molecules studied, and if so, can such tendencies have a connection to certain aspects of the species' most crucial physicochemical characteristics?

In Section 2 of this paper, we present the theoretical procedures of our calculations, and Section 3 discusses and reports our results. Finally, in Section 4, conclusions are drawn from the present investigation.

2 Theoretical methodology

The spherical complex optical potential (SCOP) and complex scattering potential ionisation contribution (CSP-ic) methods have been extensively employed to calculate both electron[37–43] and positron[44–47] scattering cross sections for a wide range of molecules over a broad energy spectrum, generally from ionisation potential (IP) to 5 keV for electrons and 1 eV to 5 keV for positrons, respectively. Therefore, we will only briefly reiterate the most important aspects of these approaches here. Table 1 presents a comprehensive summary of the key characteristics of the targets employed in this computational analysis. For $HCOPH_2$, we construct the molecule in Avogadro[48] and perform initial structure optimization using the MMFF94 force field. The optimization of the molecular geometry was carried out using ORCA 5.0.1 (ref. 49) molecular modeling software, with Avogadro's coordinates utilized as the input for the quantum mechanical calculations.

In SCOP formalism, the complex spherical potential is commonly described as,

Table 1 Physicochemical properties of the targets studied

Target	Ionisation potential IP (eV)	Ps formation threshold Δ_p (eV)	Dipole polarizability α (a.u.)	Dipole moment μ (D)
HCOH[50]	10.885	4.085	18.69	2.410
HCOOH[50]	11.330	4.53	22.40	1.58
$HCONH_2$ (ref. 50)	10.160	3.36	27.53	3.98
CH_3COCH_3 (ref. 50)	10.650	3.85	34.75	1.812
$HCONHCH_3$ (ref. 50)	9.830	3.03	39.12	4.041
CH_3COOH[50]	9.703	2.903	42.31	3.086
$HCOPH_2$ (ref. 48 and 49)	9.515	2.715	44.34	2.30

$$V_{opt} = V_s + V_p + iV_a \quad (1)$$

In eqn (1), the real part defines the elastic scattering channel and confines the electrostatic (V_s) and polarisation (V_p) interactions. The imaginary component, V_a, represents all the inelastic channels considered for flux absorption from the incident positron beam. Because of this last term in eqn (1), the optical potential method generates complex phase shifts δ_l. This permits the computation of the DCSs as well as integral cross sections for inelastic and elastic scattering. The static potential (V_s) is calculated using the charge density provided by Hartree–Fock (HF) atomic wavefunctions.[51] When performing calculations involving e^+ – scattering, the selection of the polarisation potential (V_p) is of utmost significance because of its significant contribution to the elastic channel during the e^+ – interaction. In the near-target region, V_p should approach the short-range correlation part $v_{co}(r)$ and will have its asymptotic form at large values of r. So here, we use Zhang *et al.*'s[52] model potential to take care of the V_p, which is given as:

$$V_{pco}(r) = -\alpha/2\ (r^2 + {r_{co}}^2)^2 \quad (2)$$

where r_{co} can be determined by taking $V_{pco}(0) = -\alpha/2{r_{co}}^4 = v_{co}(0)$. Selecting r_{co} in this manner assures that at the origin, $V_{pco}(r)$ equals $v_{co}(r)$, and near-target region, it approaches $v_{co}(r)$. In addition, for large r, it gradually converges to the correct asymptotic form $-\alpha/2r^4$ and also incorporates various non-adiabatic and multipole modifications in the intermediate region. For $v_{co}(r)$, the form provided by Perdew and Zunger[53] is utilized:

$$v_{co}(r) = \begin{cases} 0.0311 \ln r_s - 0.0584 + 0.00133 r_s \ln r_s - 0.0084 r_s, & \text{at } r_s < 1 \\ \dfrac{\gamma\left(1 + \frac{7}{6}\beta_1 {r_s}^{1/2} + \frac{4}{3}\beta_2 r_s\right)}{\left(1 + \beta_1 {r_s}^{1/2} - \beta_2 r_s\right)^{-2}}, & \text{at } r_s \geq 1 \end{cases} \quad (3)$$

where $r_s = \sqrt[3]{\dfrac{3}{4\pi\rho(r)}}$ represents the density parameter, $\rho(r)$ is the target charge density, and the constants γ, β_1, and β_2 have the respective values of −0.1423, 1.0523, and 0.3334.

While the absorption potential (V_a) is accountable for Ps formation, electronic excitations, and direct ionisation. For e^+ – scattering, the definition of the threshold for absorption (Δ) to start becomes a bit contentious. The depiction of the Ps formation channel is challenging, as it constitutes the predominant channel for inelastic scattering that typically opens in an electronic state with an energy lower than the first excited one. Since the formation of the Ps channel cannot be defined through binary collisions, it is impossible to include it explicitly in the original version of the absorption potential as a separate inelastic process. As a result, Reid and Wadehra[54] proposed utilizing the energy (Δ_p) required for Ps formation as the parameter for absorption threshold (Δ). The Q_{total} at higher energies was shown to be slightly overestimated by this method. Hence, we have utilized the phenomenological technique proposed by Chiari *et al.*,[55] however, in a modified form because their approach fails to accurately depict the pathway *via* which Ps is formed. To overcome this limitation, we employed the target's IP in the Δ expression. The modified form of the Δ can be written as:

$$\Delta(E) = \mathrm{IP} - (\mathrm{IP} - \Delta_p)\exp\frac{-(E_i - \Delta_p)}{E_m} \quad (4)$$

In the above eqn (4), Δ_p is the Ps formation threshold energy, and the characteristic energy denoted by E_m corresponds to the energy level at which the absorption potential (V_a), in the absence of Ps formation, yields the highest cross section. The inverse exponential function shift within the specified constraints, $\Delta(E) = \Delta_p$ for energies spanning the Ps formation energy, and for larger energies, $\Delta(E) = \mathrm{IP}$, is modulated by E_m.

As previously mentioned, Q_{inel} obtained by using eqn (4) contains channels such as electronic excitation, Ps formation, and ionisation of the target. Thus, the Q_{inel} is obtained as,

$$Q_{inel}(E_i) = Q_{ion}(E_i) + Q_{ps}(E_i) + \sum Q_{exc}(E_i) \quad (5)$$

where $Q_{ion}(E_i)$ is the sum of all permissible direct ionisation cross sections, $Q_{ps}(E_i)$ is the Ps formation cross section, and $\sum Q_{exc}(E_i)$ reflects the total of all discrete electronic excitation cross sections across all available states. A new term, Q_{in} is defined in such a way that,

$$Q_{in}(E_i) = Q_{ion}(E_i) + \sum Q_{exc}(E_i) = Q_{inel}(E_i) - Q_{ps}(E_i) \quad (6)$$

Starting from this point of reference, the modified form of the CSP-ic method (refer to ref. 45–47 for more details) can be utilized in its typical form to establish Q_{ion} from Q_{in}. The estimation error for the direct ionisation cross section is roughly 7% with the current approach. Now, we may calculate the total ionisation cross section by summing the cross sections for direct ionisation (Q_{ion}) and Ps formation (Q_{ps}), given as

$$Q_{totalion}(E_i) = Q_{ion}(E_i) + Q_{ps}(E_i) \quad (7)$$

3 Results and discussion

3.1 Comparative analysis of total cross sections (TCSs)

Fig. 1(a) shows the energy dependencies of Q_{total} (with and without Q_{ps}) for $HCONH_2$, $HCOPH_2$, and HCOOH over a wide energy range (1 eV to 5 keV). Since some models in the literature do not explicitly account for Ps formation, we have reported both TCSs for comparison. Notably, including such channels, especially for positronium, which is intrinsically multi-centered, would be computationally expensive and extremely challenging. In this figure, we also present the experimental Q_{total} results for formic acid from Kimura *et al.*,[29] Makochekanwa *et al.*,[30] and Zecca *et al.*[31] For its isoelectronic system, formamide, elastic integral cross sections from Silva *et al.*[35] are included. Except for Makochekanwa *et al.*,[30] the experimental results have not been corrected for forward scattering effects. The trend of the Q_{total} as a function of energy for each target is quite apparent; specifically, the magnitude of the Q_{total} decreases as the positron impact energy (E_i) increases until their respective Ps formation thresholds (see Table 1) are reached. With the opening of the Ps formation (Δ_p) channel, the slope of the Q_{total} changes dramatically so that its magnitude at higher energy virtually plateaus. Above Δ_p, the direct ionisation and electronic-state channels gradually open, contributing to the plateau in Q_{total} observed in each target.

For e^+ – formic acid scattering, Q_{total} reported by Zecca *et al.*[31] exhibits behavior consistent with the present Q_{total} (without Q_{ps}) with a magnitude comparable to the former; however, below the Ps formation threshold at $\Delta_p = 4.53$ eV, present results are significantly lower than the latter, while above this range, the relationship reverses as compared to Q_{total} (with Q_{ps}); when its magnitude increases due to the growing impact of the Ps formation and other inelastic channels. This behavior is in contrast to the agreement observed with the results of Kimura *et al.*[29] and Makochekanwa *et al.*,[30] which is reasonable below 4.53 eV. We have also plotted the modified results of Makochekanwa *et al.*[30] after correction for the effects of forward

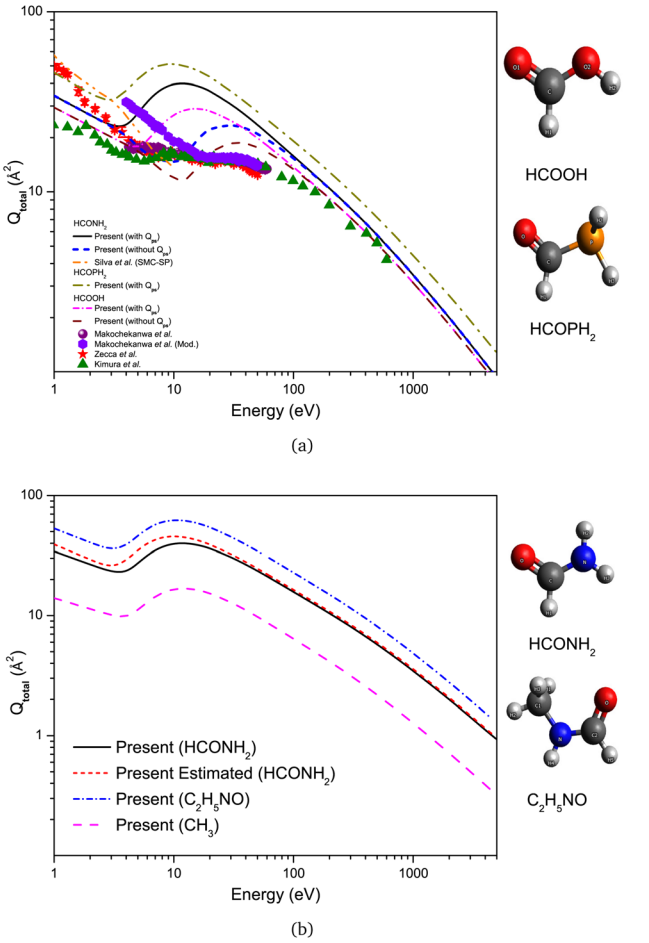

Fig. 1 Q_{total} for e^+ – scattering from (a) HCOOH, and $HCOPH_2$; (b) $HCONH_2$, and C_2H_5NO. Solid line, dash dot line, and short dash dot line: present Q_{total} (with Q_{ps}); short dash line and dash line: present Q_{total} (without Q_{ps}); dash dot dot line: Silva *et al.*;[35] solid triangles: Kimura *et al.*;[29] solid circles and solid hexagon: Makochekanwa *et al.*;[30] solid stars: Zecca *et al.*[31]

scattering that become negligible above 15 eV. At intermediate energies, the present Q_{total} (with Q_{ps}) runs distinctly above the experimental results but is lower in magnitude than the corrected results of Makochekanwa *et al.*[30] below 7 eV while being in very good agreement with those of Kimura *et al.*[29] at all overlap energies above 100 eV. The experimental data's lack of angular resolution adjustment is generally responsible for the discrepancy in results. When the effects of the Ps formation are not included, the disparity between the curves becomes much less pronounced throughout the entire energy range.

For the e^+ – formamide scattering shown in Fig. 1(a), the present Q_{total} (without Q_{ps}) results differ quantitatively and qualitatively from the SMC results of Q_{el} from Silva *et al.*[35] Their results are consistently higher in magnitude, with the difference increasing with decreasing E_i, amounting to a minimum of 4% at 10 eV to a maximum of around 40% at 1 eV. On the contrary, above $\Delta_p = 3.36$ eV, we do not anticipate a positive correspondence between Q_{total} (with Q_{ps}) and SMC results, as the authors have not considered the Ps formation, so their results exhibit

lower values in comparison to our results. However, the discrepancies observed between the present results and their calculations below the Ps formation threshold cannot be explained solely through contributions from inelastic channels.

Since no experimental or theoretical Q_{total} for e^+ – scattering from formamide is available in the literature, we compare the present results with the calculated and measured Q_{total} of formic acid. Formamide differs from formic acid with the substitution of a OH group instead of NH_2. Hence, comparing the cross-sectional results of these two systems will be interesting. It is clear from Fig. 1(a) that the present e^+ – formamide data are, on average, greater in magnitude than the formic acid results, with a maximum difference of around 32% at their respective maxima points. Some of this behavior could be explained by formamide being a larger compound than formic acid, but more likely, this is due to the higher dipole polarisability (α) and dipole moment (μ) of formamide compared to that of formic acid. For $HCONH_2$, present Q_{total} monotonically decreases as the positron impact energy increases from 1 eV ($\sim 34.236 \times 10^{-20}$ m^2) until around the Ps formation threshold ($\sim 22.878 \times 10^{-20}$ m^2), and thereafter, the Q_{total} increases, reaching its maximum ($\sim 40.024 \times 10^{-20}$ m^2) at 12 eV, before decreasing again until the highest energy of 5000 eV ($\sim 0.931 \times 10^{-20}$ m^2). A similar trend is observed for HCOOH, starting from 1 eV ($\sim 29.439 \times 10^{-20}$ m^2) and attaining its first minima around $\Delta_p = 4.53$ eV ($\sim 17.45 \times 10^{-20}$ m^2) and then maxima at 15 eV ($\sim 28.972 \times 10^{-20}$ m^2) before finally declining at 5 keV ($\sim 0.866 \times 10^{-20}$ m^2).

Similarly, there is no experimental or theoretical literature available for e^+ – $HCOPH_2$ scattering that we can use to benchmark against the current positron TCSs. So, we further conduct a comparative analysis of $HCOPH_2$ results with $HCONH_2$. For $HCOPH_2$, Q_{total} decreases sharply from 1 eV ($\sim 45.903 \times 10^{-20}$ m^2) to around $\Delta_p = 2.715$ eV ($\sim 31.033 \times 10^{-20}$ m^2) until it reaches its maximum value at 9 eV ($\sim 51.205 \times 10^{-20}$ m^2) ultimately diminishing at 5 keV ($\sim 1.275 \times 10^{-20}$ m^2). $HCOPH_2$ results are uniformly larger in magnitude than the corresponding $HCONH_2$ results, with a difference of about 27% at 1 eV, decreasing with increasing E_i to a maximum of 24% at their maximum energy points. Even though $\alpha_{HCOPH_2} \gg \alpha_{HCONH_2}$, this percentage reflects a small difference between these targets' respective maxima points as compared to the difference observed in HCOOH and $HCONH_2$ results, which is explained in terms of a "compensation effect" caused by $\mu_{HCONH_2} > \mu_{HCOPH_2}$. The relationship between the target's physicochemical properties and the respective cross section is not surprising. It is widely recognized that the properties of the target molecule significantly affect the scattering dynamics in e^+ scattering systems.[56–59] Therefore, when comparing the behavior of different targets, both of these long-range interactions are very important.[60,61]

Fig. 1(b) shows that the Q_{total} for $HCONH_2$ can be roughly estimated from the subtraction of Q_{total} for the $HCONHCH_3$ molecule and one methyl unit, CH_3, and the obtained Q_{total} shows good agreement with the present calculated results of $HCONH_2$, especially for energies above 10 eV. The disagreement estimated in this manner and the measured Q_{total} for $HCONH_2$ at lower positron impact energies are related to the fact that the straightforward subtraction of the Q_{total} for constituents does not account for the change in charge-density distribution that occurs for methylation.

In Fig. 2, we present the results of our Q_{total} (with and without Q_{ps}) measurements from e^+ – scattering from acetone and acetic acid, along with the experimental and theoretical results accessible in the literature.[21,29,32,33] For e^+ – acetone scattering, we observe that the results of Zecca *et al.*[32] exhibit strong consensus to the present Q_{total} (without Q_{ps}), with a magnitude considerably smaller for energies above 10 eV. On the other hand, the Q_{total} reported by Hamada *et al.*[33] and Kimura *et al.*,[29] show divergent behavior below 2 eV, despite good agreement above this energy. Within the Ps formation threshold at $\Delta_p = 3.85$ and 100 eV, the present Q_{total} (with Q_{ps}) shows a larger discrepancy with the experimental results, where Ps formation is responsible for around 50% of the Q_{total}. We, therefore, currently lack a quantitative clarification for this unexpected finding; we merely mention that experimental results suggest a smaller magnitude of the Q_{ps} in comparison to what is implied by the present calculations of Q_{total} and Q_{ps}. Moreover, the angular resolution of the various experimental devices explains the difference in the magnitudes of various measurements of the cross section. Due to the limited angular resolution of the experimental apparatuses, the Q_{total} does not account for precise information at smaller angles. As a result, the measured Q_{total} will underestimate the actual values. Hence, the disparities observed between the experimental measurements and the theoretical calculations for Q_{total} at low and intermediate energies can mostly be ascribed to the limited angular resolution of the experimental apparatus.

Regarding the theoretical computations from Lima *et al.*,[21] the shape of the present Q_{total} (without Q_{ps}) appears to be in reasonable agreement with these SMC results. However, below $\Delta_p = 3.85$ eV, our results diverge from their calculations as they are consistently higher in magnitude, with a difference of around 10–16%, and finally merging above 3.85 eV. The

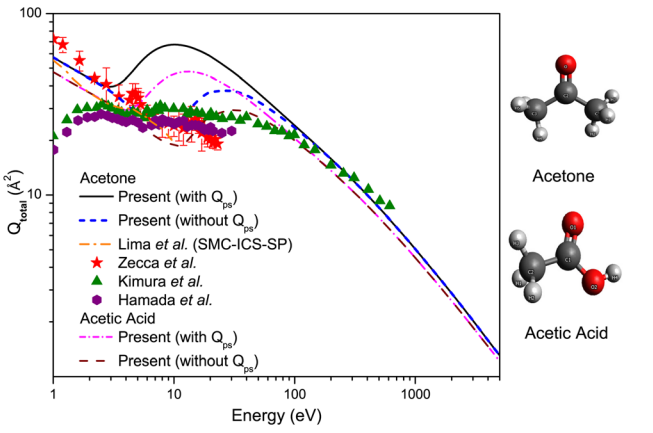

Fig. 2 Q_{total} for e^+ – scattering from acetone and acetic acid. Solid line and short dash dot line: present Q_{total} (with Q_{ps}); short dash line and dash line: present Q_{total} (without Q_{ps}); dash dot line: Lima *et al.*;[21] solid triangles: Kimura *et al.*;[29] solid stars: Zecca *et al.*;[32] solid hexagon: Hamada *et al.*[33]

disagreement below 3.85 eV is presumably due to the constraints of the different potential models applied for elastic calculations. When considering Ps formation above 3.85 eV, the difference is quite high, which is associated mainly with the underestimating of the inelastic contribution in SMC calculations, as only the elastic contributions are considered. Based on the good agreement seen from Fig. 1(a) and 2 between the present and experimental results of Kimura *et al.*[29] within the range of 100 and 600 eV, one can infer that our computations reasonably represent the Q_{total} for higher energies. Unfortunately, currently, there are no other results available for these targets in the literature, especially theoretical ones. The discrepancies between the present Q_{total} and those elastic calculations, as well as with the experimental literature, most likely indicate that further experimental and theoretical e^+ – scattering data is required for better analyses of the results.

In Fig. 2, we also compare the calculated Q_{total} of CH_3COOH at energies between 1 and 5000 eV with the present results of CH_3COCH_3. The similarity between the shapes of cross sections for these two targets suggests that replacing the OH group with CH_3 would account for most differences. At 1 eV, for CH_3COOH, the Q_{total} can be read graphically as approximately 47.558×10^{-20} m^2, which can be compared to the Q_{total} of CH_3COCH_3 around 57.262×10^{-20} m^2, *i.e.*, the difference is roughly 9.704×10^{-20} m^2, or about 18%. However, a large deviation emerges around their respective peak regions, which is found at 10 eV ($\sim 67.509 \times 10^{-20}$ m^2) for CH_3COCH_3 and 13 eV ($\sim 47.898 \times 10^{-20}$ m^2) for CH_3COOH, respectively, where Q_{total} values of CH_3COCH_3 are larger by 42%, at most, than those of CH_3COOH. At 10 eV, for CH_3COCH_3, the contribution from Q_{ps} (see Fig. 4(c)) is expected to consist of 62% of the Q_{total}, whereas Q_{el} (see Fig. 4(a)) is approximately 25.161×10^{-20} m^2, *i.e.*, around 37% of the Q_{total} and therefore, the sum of all ionisation (Q_{ion}) and electronic excitation (Q_{exc}) is considered to fill up the rest 1%. Similarly, at 13 eV for CH_3COOH, contributions from Q_{ps} and Q_{el} are expected to be around 57% and 38% of the Q_{total}, respectively, and the rest 5% corresponds to the contribution from the summation of $Q_{ion} + Q_{exc}$. As seen from Table 1, both dipole polarisability and dipole moment of CH_3COOH are larger than those of CH_3COCH_3, while the geometric dimensions in CH_3COCH_3 are bigger as compared to CH_3COOH. So, while the relative behavior of the Q_{total} might be reflected in terms of the molecule's respective α and μ, the size of the targets also plays a key role in its magnitude.

The present theoretical Q_{total} for formaldehyde, obtained in the 1–5000 eV energy range, is shown in Fig. 3, which is compared to the only other experimental results of Zecca *et al.*[34] at low and intermediate positron-impact energies. Evidently, the magnitudes of the two results differ significantly. Experimental results are higher in magnitude than the present Q_{total} (with Q_{ps}) below around 7 eV, and within 7 and 50.3 eV, their results are lower as compared to our computations. The authors also reported theoretical SMC calculations of elastic (with and without Born closure) at static and polarisation levels with a magnitude greater than their Q_{total}, which is nonphysical. Although forward angle scattering corrections were not included in their measurements, which, when accounted for, may produce an enormous rise in the magnitude of their Q_{total}, it is challenging to attribute the extensive nature of this effect. Thus, formaldehyde requires further experimental and theoretical investigations to validate our results.

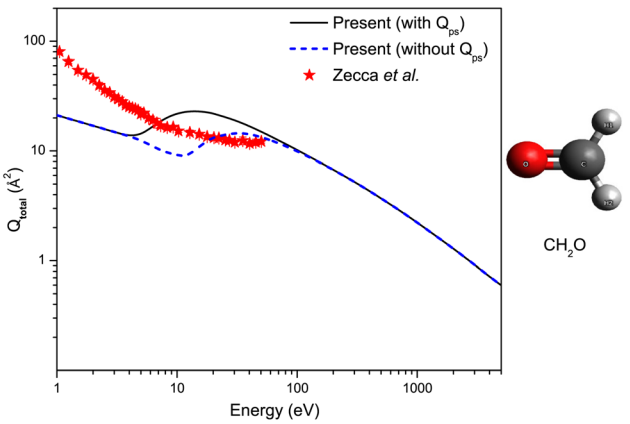

Fig. 3 Q_{total} for e^+ – scattering from formaldehyde. Solid line: present Q_{total} (with Q_{ps}); short dash line: present Q_{total} (without Q_{ps}); solid stars: Zecca *et al.*[34]

3.2 Comparative analysis of elastic and inelastic cross sections

The comparison between the elastic and inelastic cross sections calculated in this work for all seven targets using SCOP and CSP-ic approximations in the energy range 1 eV to 5 keV is presented in Fig. 4. The common energy reliance of all cross sections is very similar, and we observe a few interesting general characteristics of the current cross sections for all targets in the following manner: (i) there exists a general increase in the order of magnitude for the cross-section with the size of the molecule. For example, the most distinctive feature of the computed cross sections for the CH_3COCH_3 is their relatively high magnitude across the entire investigated energy range as compared to other targets. Such a high cross section partially reflects the molecule's large geometrical dimensions. The magnitude of the cross sections decreases in the order of CH_3COCH_3 → $HCONHCH_3$ → CH_3COOH → $HCOPH_2$ → $HCONH_2$ → $HCOOH$ → CH_2O, *i.e.*, the molecular size. (ii) Elastic cross sections start to grow at notably lower energy regions. This is a characteristic trait of polar targets.[62] Beyond the ~100 eV range, all cross sections decline at almost a constant rate, and the magnitude's order is approximately proportional to the geometric dimensions of the molecule. (iii) Inelastic cross sections possess a conspicuously prominent hump at roughly 10 eV and then gradually drop on the lower and higher energy sides. The dominating hump transitions towards higher energy regions, originating from 10 to 17 eV, as the target evolves lighter from CH_3COCH_3 → CH_2O.

The most striking aspect of these Fig. 4(a)–(f) is how qualitatively comparable the energy dependency of the cross sections is for each target in the energy domain we studied. Although there are certain distinctions as a result of the different target ionisation potentials and Ps formation thresholds, the

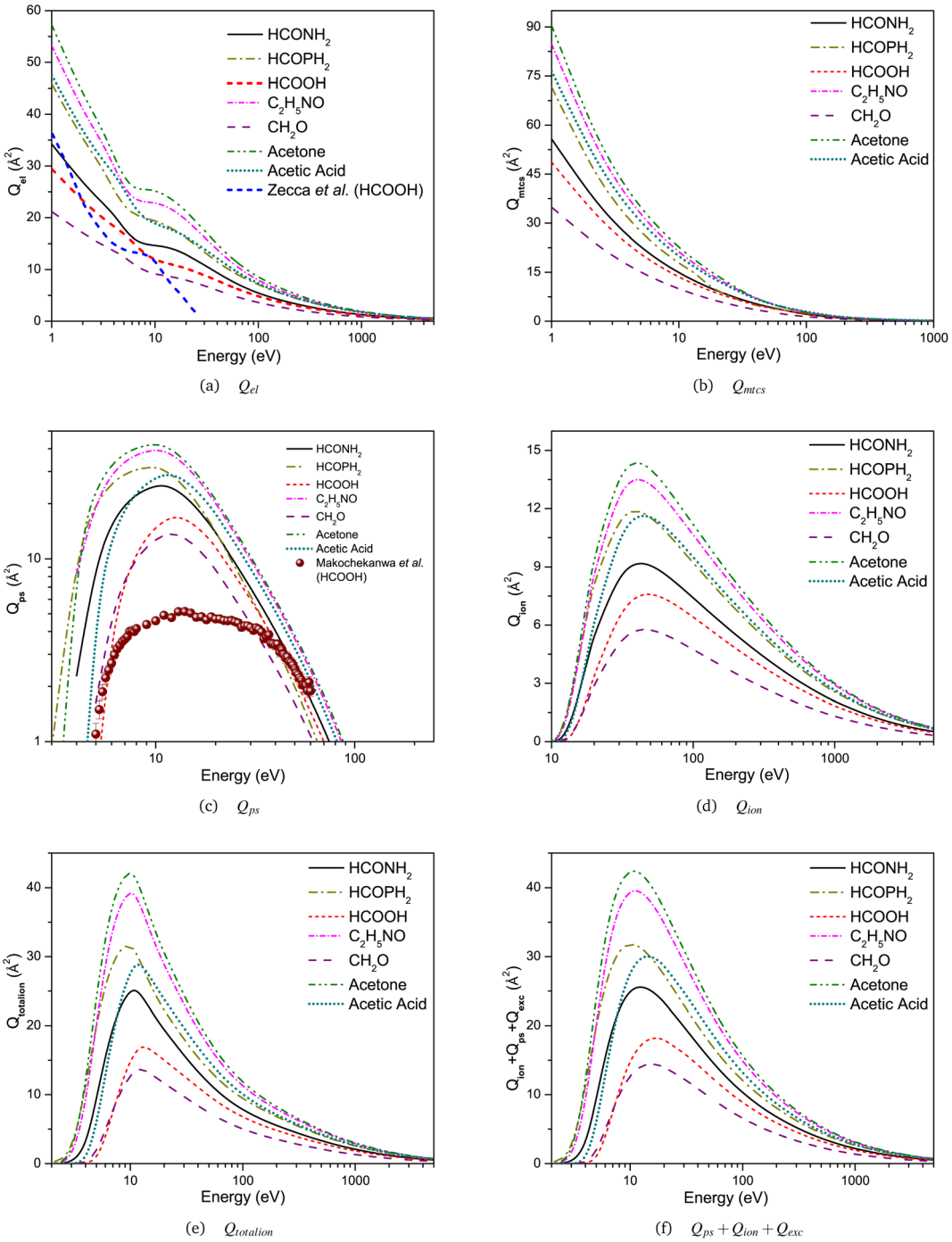

Fig. 4 (a) Q_{el}, (b) Q_{mtcs}, (c) Q_{ps}, (d) Q_{ion}, (e) $Q_{totalion}$, and (f) $Q_{ps} + Q_{ion} + Q_{exc}$ for positron scattering from $HCONH_2$, $HCOPH_2$, HCOOH, C_2H_5NO, CH_2O, acetone, and acetic acid.

similarities between the forms of the numerous cross sections are pretty remarkable. Attempting to classify these compounds according to the values of their dipole polarisabilities (see Table 1) yields a clear hierarchy between those targets with a comparatively high value (CH_3COCH_3, CH_3COOH, $HCONHCH_3$, and $HCOPH_2$ – group A), those with an intermediate value ($HCONH_2$ and HCOOH – group B), and finally, the target with a relatively low value (HCOH – group C). Regarding group A, then, we discover all of these targets also have very identical values for the α, and when we see from Fig. 4, it is also clear that, within the limitations of our computations, their cross sections likewise have remarkably similar forms and absolute magnitudes. Makochekanwa *et al.*[30] and Chiari *et al.*[59] also observed a link between dipole polarisabilities and the cross sections of molecules. A similar argument is feasible for the Group B targets. Ultimately, for HCOH, it is evident that its α is approximately fifty percent of the targets in group A, and quite interestingly, its cross section, over the majority of the

prevalent energy domain, is also around fifty percent of the group A targets.

Fig. 4(a) and (b) show the elastic and momentum transfer cross sections for the present targets, respectively. Q_{mtcs} is a valuable parameter for the MC method as well as similar simulations, which measure the average momentum transferred between the target molecules and e^+ during the elastic scattering process.[63] The general cross-sectional energy dependence of Q_{el} is identical to the Q_{total}, however, the extent is 30–40% less than that of the Q_{total}. The influence of the maximum peak witnessed in the Q_{total} due to the Ps formation at 10 to 15 eV appears to become slightly weakened in the Q_{el}, and at higher energies above 20 eV, they decline at a considerably faster rate than Q_{total} reflecting the growing importance of the inelastic channels. Although a small shoulder appears for all targets around 10 eV, it is found to be more pronounced for CH_3COCH_3 and C_2H_5NO. Fig. 4(a) also confronts the present results of formic acid and SMC computations of Zecca *et al.*[31] available in the literature for the e^+ – scattering. It is apparent that, at least in the context of 1–25 eV, where the energies of SMC computations and our SCOP method overlap, their curves that symbolize elastic integral cross section lie systematically below the present results at all energies except below 2 eV. The variations between the SMC values and the present calculated Q_{el} reach about 22% around 4 eV, less than 1% at 10 eV, and show a maximum deviation of more than about 80% around 25 eV.

Fig. 4(c)–(f) show inelastic cross sections for all targets. Unfortunately, to our knowledge, theoretical or experimental inelastic cross sections for e^+ – scattering by most of the present targets have not been reported in the literature yet. So, the present results appear to be novel. Above a few tens of eV, Q_{ps} is anticipated to become predominant, constituting the majority of the Q_{total}. The difference between the Q_{total} and Q_{ps} provides details about the sum of Q_{el} and other Q_{inel} (Q_{ion} and Q_{exc}) processes. Amongst all inelastic channels, Ps formation and ionisation should predominantly become the primary contributors between the energy range of 5 and 100 eV. The Ps formation function appears to fade above ~150 eV, where the cross section is approaching zero. But, approximately above the ~100 eV energy, it is comparatively smaller, as anticipated.

We also plot the present calculated Q_{ps} in Fig. 4(c), along with the only available experimental measurements of Ps formation cross section from Makochekanwa *et al.*[30] for e^+ – HCOOH scattering. We observe that the present Q_{ps} starts rising sharply at around the Ps formation threshold at $\Delta_p = 4.53$ eV, and then peaks at 13 eV ($\sim 16.823 \times 10^{-20}$ m^2) before its magnitude begins to decrease as the positron energy increases. The sole element of genuine agreement between the experimental and our theoretical results would seem to be the location of the maximum of the Q_{ps} at around 13 eV for our calculations and about 14 eV for the experimental measurements. Makochekanwa *et al.*[30] results exhibit an abrupt increase in the cross section up to 14 eV and then a relatively flat peak region, with a magnitude close to $\sim 5.149 \times 10^{-20}$ m^2 that expands to around 25 eV prior to a progressive decrease to approximately $\sim 1.889 \times 10^{-20}$ m^2 at 60 eV. We are not familiar with any further reports on the measurement or calculation of the Q_{ps} and other inelastic cross sections for these seven targets studied. So, a more in-depth and comprehensive understanding should wait for a better-detailed joint experimental and theoretical investigation.

4 Conclusions

This study systematically analyzes elastic and inelastic cross sections for e^+ – scattering from a category of organic molecules that function like biological "moieties" or "sub-units" to the nucleotides. A good qualitative agreement, especially below and above the opening of the Ps formation channel, was found between the experimental and present theoretical TCSs, with this comparison emphasizing the critical role played by both dipole polarizability (α) and the permanent dipole moment (μ) of molecules in the scattering process. The present targets are polar molecules with reasonably high α; we believe that the observed energy dependence of the cross sections strongly correlates with the intrinsic physicochemical properties of their target molecules. Specifically, the long-range dipole interaction is primarily driven by α, which could be powerful enough to dominate the static interaction and significantly influence the scattering dynamics at low energies. Except for a few, neither experimental nor theoretical investigations on e^+ – scattering exist for these seven targets. So, the present work is the first systematic research work carried out on these targets. We hope that this work will inspire further experimental and theoretical research into positron collision studies and serve as a contribution to the researchers who are interested in this topic.

Conflicts of interest

There are no conflicts to declare.

References

1 C. Makochekanwa, O. Sueoka and M. Kimura, *J. Chem. Phys.*, 2003, **119**, 12257–12263.
2 C. Makochekanwa, H. Kato, M. Hoshino, M. H. F. Bettega, M. A. P. Lima, O. Sueoka and H. Tanaka, *J. Chem. Phys.*, 2007, **126**, 164309.
3 K. J. H. George, S. Borjian, M. C. Cross, J. W. Hicks, P. Schaffer and M. S. Kovacs, *RSC Adv.*, 2021, **11**, 31098–31123.
4 E. Campbell, C. Jordan and R. Gilmour, *Chem. Soc. Rev.*, 2023, **52**, 3599–3626.
5 M. Kimura, O. Sueoka, C. Makochekanwa, H. Kawate and M. Kawada, *J. Chem. Phys.*, 2001, **115**, 7442–7449.
6 G. F. Gribakin, J. A. Young and C. M. Surko, *Rev. Mod. Phys.*, 2010, **82**, 2557.
7 J. Hofierka, B. Cunningham, C. M. Rawlins, C. H. Patterson and D. G. Green, *Nat*, 2022, **606**, 688–693.
8 A. Zecca, E. Trainotti, L. Chiari, M. H. F. Bettega, S. D. Sanchez, M. T. D. N. Varella, M. A. P. Lima and M. J. Brunger, *J. Chem. Phys.*, 2012, **136**, 124305.

9 S. Falcinelli, F. Vecchiocattivi, B. G. Brunetti, M. Parriani, G. Gigliotti, S. Stranges and F. Pirani, *RSC Adv.*, 2022, **12**, 7587–7593.
10 B. Boudaıffa, P. Cloutier, D. Hunting, M. A. Huels and L. Sanche, *Sci*, 2000, **287**, 1658–1660.
11 J. A. Sabin del Valle and F. A. Gianturco, *Phys. Chem. Chem. Phys.*, 2005, **7**, 318–325.
12 M. Pietrow, R. Zaleski, A. Wagner, P. Słomski, E. Hirschmann, R. Krause-Rehberg, M. O. Liedke, M. Butterling and D. Weinberger, *Phys. Chem. Chem. Phys.*, 2021, **23**, 11264–11271.
13 M. Šuvakov, Z. L. Petrović, J. P. Marler, S. J. Buckman, R. E. Robson and G. Malović, *New J. Phys.*, 2008, **10**, 053034.
14 J. P. Marler, Z. L. Petrović, A. Banković, S. Dujko, M. Šuvakov, G. Malović and S. J. Buckman, *Phys. Plasmas*, 2009, **16**, 057101.
15 M. C. Fuss, A. Muñoz, J. C. Oller, F. Blanco, M.-J. Hubin-Franskin, D. Almeida, P. Limão-Vieira and G. García, *Chem. Phys. Lett.*, 2010, **486**, 110–115.
16 A. Muñoz, F. Blanco, G. Garcia, P. A. Thorn, M. J. Brunger, J. P. Sullivan and S. J. Buckman, *Int. J. Mass Spectrom.*, 2008, **277**, 175–179.
17 A. Kumar, P. Sharma, N. Sharma, Y. Kumar and D. Mahajan, *RSC Adv.*, 2021, **11**, 25777–25787.
18 D. Bockelée-Morvan, D. C. Lis, J. E. Wink, D. Despois, J. Crovisier, R. Bachiller, D. J. Benford, N. Biver, P. Colom, J. K. Davies, *et al.*, *Astron. Astrophys.*, 2000, **353**, 1101–1114.
19 W. A. Schutte, A. C. A. Boogert, A. G. G. M. Tielens, D. C. B. Whittet, P. A. Gerakines, J. E. Chiar, P. Ehrenfreund, J. M. Greenberg, E. F. Van Dishoeck, T. Graauw, *et al.*, *Astr. Ap.*, 1999, **343**, 966–976.
20 R. Frigge, C. Zhu, A. M. Turner, M. J. Abplanalp, B.-J. Sun, Y.-S. Huang, A. H. H. Chang and R. I. Kaiser, *Chem. Commun.*, 2018, **54**, 10152–10155.
21 R. O. Lima, G. M. Moreira, M. H. F. Bettega and S. D. Sanchez, *J. Phys. Chem. A*, 2020, **124**, 6790–6793.
22 F. F. Da Silva, M. Nobre, A. Fernandes, R. Antunes, D. Almeida, G. Garcia, N. J. Mason and P. Limão-Vieira, *J. Phys.: Conf. Ser.*, 2008, 012011.
23 Y. Yamada, Y. Kita and M. Tachikawa, *Phys. Rev. A*, 2014, **89**, 062711.
24 P. Możejko, S. Stefanowska-Tur, E. Ptasińska-Denga and C. Szmytkowski, *J. Chem. Phys.*, 2019, **151**, 064305.
25 H. Bhutadia, M. Vinodkumar and B. Antony, *J. Phys.: Conf. Ser.*, 2012, 052071.
26 D. Gupta, R. Naghma and B. Antony, *Mol. Phys.*, 2014, **112**, 1201–1209.
27 D. Gupta, R. Naghma and B. Antony, *AIP Adv.*, 2015, **5**, 097159.
28 C. Limbachiya, A. Chaudhari, H. Desai and M. Vinodkumar, *RSC Adv.*, 2015, **5**, 103964–103976.
29 M. Kimura, O. Sueoka, A. Hamada and Y. Itikawa, *Adv. Chem. Phys.*, 1999, 537–622.
30 C. Makochekanwa, A. Bankovic, W. Tattersall, A. Jones, P. Caradonna, D. S. Slaughter, K. Nixon, M. J. Brunger, Z. Petrovic, J. P. Sullivan, *et al.*, *New J. Phys.*, 2009, **11**, 103036.
31 A. Zecca, L. Chiari, A. Sarkar, M. A. P. Lima, M. H. F. Bettega, K. L. Nixon and M. J. Brunger, *Phys. Rev. A*, 2008, **78**, 042707.
32 A. Zecca, L. Chiari, E. Trainotti, A. Sarkar and M. J. Brunger, *PMC Phys. B*, 2010, **3**, 1–7.
33 A. Hamada, O. Sueoka, H. Takaki and M. Kimura, *Bull. Phys. Soc. Jpn.*, 1997, **52**, 876.
34 A. Zecca, E. Trainotti, L. Chiari, G. García, F. Blanco, M. H. F. Bettega, M. T. do N Varella, M. A. P. Lima and M. J. Brunger, *J. Phys. B: At., Mol. Opt. Phys.*, 2011, **44**, 195202.
35 M. O. Silva, G. M. Moreira, M. H. F. Bettega and S. d. Sanchez, *J. Phys. Chem. A*, 2020, **124**, 6009–6015.
36 W. Tattersall, L. Chiari, J. R. Machacek, E. Anderson, R. D. White, M. J. Brunger, S. J. Buckman, G. Garcia, F. Blanco and J. P. Sullivan, *J. Chem. Phys.*, 2014, **140**, 044320.
37 S. Mahla, P. Modak and B. Antony, *J. Phys. Chem. A*, 2023, **127**, 5414–5423.
38 B. Goswami and B. Antony, *RSC Adv.*, 2014, **4**, 30953–30962.
39 B. Goswami, R. Naghma and B. Antony, *RSC Adv.*, 2014, **4**, 63817–63823.
40 D. Gupta, R. Naghma, B. Goswami and B. Antony, *RSC Adv.*, 2014, **4**, 9197–9204.
41 J. Kaur, R. Naghma and B. Antony, *RSC Adv.*, 2015, **5**, 20090–20097.
42 M. Vinodkumar, C. Limbachiya, H. Desai and P. C. Vinodkumar, *RSC Adv.*, 2015, **5**, 69466–69478.
43 M. Vinodkumar, H. Desai and P. C. Vinodkumar, *RSC Adv.*, 2015, **5**, 24564–24574.
44 S. Mahla and B. Antony, *J. Appl. Phys.*, 2023, **134**, 124901.
45 N. Sinha, P. Modak, S. Singh and B. Antony, *J. Phys. Chem. A*, 2018, **122**, 2513–2522.
46 S. Singh, S. Dutta, R. Naghma and B. Antony, *J. Phys. Chem. A*, 2016, **120**, 5685–5692.
47 N. Sinha, A. K. Sahoo and B. Antony, *J. Phys. Chem. A*, 2020, **124**, 5147–5156.
48 M. D. Hanwell, D. E. Curtis, D. C. Lonie, T. Vandermeersch, E. Zurek and G. R. Hutchison, *J. Cheminf.*, 2012, **4**, 17.
49 F. Neese, F. Wennmohs, U. Becker and C. Riplinger, *J. Chem. Phys.*, 2020, **152**, 224108.
50 CCCBDB, *Computational Chemistry Comparison and Benchmark Database*, 2023, **https://cccbdb.nist.gov/**, (accessed April 2, 2023).
51 H. L. Cox Jr. and R. A. Bonham, *J. Chem. Phys.*, 1967, **47**, 2599–2608.
52 X. Zhang, J. Sun and Y. Liu, *J. Phys. B*, 1992, **25**, 1893.
53 J. P. Perdew and A. Zunger, *Phys. Rev. B: Condens. Matter Mater. Phys.*, 1981, **23**, 5048–5079.
54 D. D. Reid and J. M. Wadehra, *J. Phys. B: At., Mol. Opt. Phys.*, 1996, **29**, L127.
55 L. Chiari, A. Zecca, S. Girardi, E. Trainotti, G. Garcia, F. Blanco, R. P. McEachran and M. J. Brunger, *J. Phys. B: At., Mol. Opt. Phys.*, 2012, **45**, 215206.
56 P. Palihawadana, R. Boadle, L. Chiari, E. K. Anderson, J. R. Machacek, M. J. Brunger, S. J. Buckman and J. P. Sullivan, *Phys. Rev. A*, 2013, **88**, 012717.
57 A. Zecca, L. Chiari, A. Sarkar, K. L. Nixon and M. J. Brunger, *Phys. Rev. A*, 2008, **78**, 022703.

58 M. J. Brunger, S. J. Buckman and A. Zecca, *J. Phys.: Conf. Ser.*, 2009, **194**, 012034.
59 L. Chiari, A. Zecca, E. Trainotti, M. H. F. Bettega, S. d. Sanchez, M. T. d. N. Varella, M. A. P. Lima and M. J. Brunger, *Phys. Rev. A*, 2013, **87**, 032707.
60 L. Chiari, A. Zecca, F. Blanco, G. García and M. J. Brunger, *J. Phys. B: At., Mol. Opt. Phys.*, 2014, **47**, 175202.
61 L. Chiari, A. Zecca, E. Trainotti, G. Garcia, F. Blanco, M. H. F. Bettega, S. d. Sanchez, M. T. d. N. Varella, M. A. P. Lima and M. J. Brunger, *Phys. Rev. A*, 2013, **88**, 022708.
62 L. Chiari, A. Zecca, F. Blanco, G. García and M. J. Brunger, *Phys. Rev. A*, 2015, **91**, 012711.
63 N. A. Mori, L. H. Scarlett, I. Bray and D. V. Fursa, *Phys. Rev. A*, 2023, **107**, 032817.